



Preparation and characterization of ZnO/Chitosan nanocomposite for Cs(I) and Sr(II) sorption from aqueous solutions

G. A. Dakroury¹ · E. A. A. El-Shazly¹ · H. S. Hassan²

Received: 15 May 2021 / Accepted: 31 July 2021 / Published online: 16 August 2021
© Akadémiai Kiadó, Budapest, Hungary 2021

Abstract

1:1 ZnO/Chitosan nanocomposite (nZnOCS nanocomposite) successfully prepared by sol–gel method and used as a sorbent for Cs(I) and Sr(II). The prepared samples characterized by different analytical techniques as FTIR, SEM, TEM, XRD, particle size analyzer, TGA/DTA, and pore size distribution. Optimization of pH of the medium, contact time, initial metal ion concentration and temperature for the sorption reaction performed. The sorption reaction kinetics follows pseudo-2nd order. The monolayer capacities at 298 K are 253.81 and 116.1 mgg⁻¹ for Cs(I) and Sr(II), respectively. The sorption process is spontaneous and endothermic.

Keywords Cs(I) · Sr(II) · Sorption · ZnO nanoparticles · Chitosan · Nanocomposite

Introduction

There has been an increase in the release of radioactive waste into the environment as a result of the expansion of the peaceful application of nuclear energy and radioactive materials in numerous industries such as medicine, agriculture, industry, and nuclear weapons [1, 2]. Long half-lives, high radiation toxicity, high solubility, and facile assimilation by organs characterise these hazardous radioactive wastes [1, 3].

Many researchers are frantically trying to discover a way to dispose of this hazardous waste. ¹³⁷Cs for example, with half life 30.1 years, has a smaller hydrated radius and higher diffusion coefficient. It can be deposited in the soft tissues throughout body and induce thyroid cancer. ⁹⁰Sr is the beta emission and its half-life is more than 28 years. It is bone- and teeth-seeking radionuclide and causes leukemia, bone sarcoma, and other chronic problems [4, 5].

Several technical methods such as; chemical precipitation, coagulation, sorption, ion exchange, and membrane technologies, applied to treat the radioactive wastewater [6–8]. Among these methods, sorption is the superior applied method because it is simple, economical, and feasible [9].

In sorption process, inorganic, organic, and biological sorbents could be used. The cost, efficiency, and environmental safety of sorbents are all factors to consider. Chitosan (CS) is a low-cost natural polymer with excellent hydrophilicity, biocompatibility, biodegradability, non-toxicity, and waste treatment activity [10]. The presence of amino and hydroxyl functional groups raise its ability for sorption. Recently, hybrid materials based on chitosan have been developed for waste treatment due to its mechanical properties as polymers, metal and metal oxide nanoparticles [11–14].

ZnO is consider a reasonable sorbent due to its low-cost and non-toxic. Both cationic dyes (malachite green (MG) and anionic dyes (acid fuchsin (AF), Congo red (CR)) were removed from aqueous solutions using ZnO nanoparticles [15]. For MG, AF, and CR, the highest sorption capacity is 2963, 3307, and 1554 mgg⁻¹, respectively. Khorsand Zak et al. [16] use a sol–gel method to make nano zinc oxide. Starch stabilises ZnO nanoparticles and reduces their size by decreases agglomeration.

Although, many authors had studied the preparation and the characterization of ZnO/Chitosan nanocomposite

✉ E. A. A. El-Shazly
ehabelshazly2010@hotmail.com

¹ Nuclear Chemistry Department, Radioisotopes Production and Radiation Sources Division, Hot Laboratories Centre, Egyptian Atomic Energy Authority, P.O. 13759, Cairo, Egypt

² Waste Management Department, Hot Laboratories Centre, Egyptian Atomic Energy Authority, P.O. 13759, Cairo, Egypt

[17–22] but it still a limitation in the study of the use of ZnO/Chitosan for the sorption of some radioactive nuclei as Cs(I) and Sr(II) metal ions.

This work concerns with the preparation of ZnO/Chitosan nanocomposite (nZnOCS). A characterization of nZnOCS nanocomposite carried out by FTIR, SEM, TEM, XRD, the particle size analyzer, TGA/DTA, and the pore size distribution. Sorption of Cs(I) and Sr(II) ions onto nZnOCS nanocomposite is explained. Basic parameters effect such as; pH, the temperature, contact time and initial metal ion concentration on metal ions discussed. Kinetics and isotherms models fitting as well as thermodynamic nature have been studied for mechanism.

Experimental

Chemicals and reagents

All the reagents are of analytical grade (i.e., purity higher than 99.9%) and used without further purification. Zinc nitrate hexahydrate $[\text{Zn}(\text{NO}_3)_2 \cdot 6\text{H}_2\text{O}]$ (M. Weight: 297.49, Sigma–Aldrich) was used as a zinc source, NaOH pellets (El-Nasr Co. (ADWIC), (Egypt) was used for hydrolysis and formation of $\text{Zn}(\text{OH})_2$. Starch purchased from Sigma–Aldrich. Metal salts of CsCl (Merk) and $\text{Sr}(\text{NO}_3)_2$ (Sigma–Aldrich) was used to prepare Cs(I) and Sr(II) solution, respectively. The stock solution (350 mgL^{-1}) was prepared by dissolving appropriate amounts of metal salts in double distilled water. The working solution (200 mgL^{-1}) was prepared by diluting the stock solution to appropriate volume. For all experiments, double distilled water was used for the preparation.

Preparation zinc oxide

Zinc oxide is prepared by two different methods; the first one hydrolysis of zinc nitrate by NaOH and the second is sol–gel method in presence of starch as stabilizer.

Preparation using zinc nitrates as precursor (ZnO) [23]

1.894 g of zinc nitrate (0.1 molL^{-1}) is dissolved in 100 mL distilled water and stirred for 30 min. 100 mL of 0.2 molL^{-1} NaOH is added drop wise to the aqueous zinc nitrates solution. The mixture is vigorously stirring for 24 h. A large amount of white precipitate was formed, this precipitate was filtered and washed with distilled water and dried at $100 \text{ }^\circ\text{C}$ for a day and milled before calcinations $600 \text{ }^\circ\text{C}/2 \text{ h}$ with a heating rate $10 \text{ }^\circ\text{C}/\text{min}$.

Preparation of nano ZnO using starch as stabilizer (nZnO) [16]

5 g of starch dissolved in 75 mL of distilled water at $75 \text{ }^\circ\text{C}$ and stirred for 0.5 h till a starch cloudy solution. In another solution 11.25 g of zinc nitrates were dissolved in 25 mL of distilled water and stirred for 0.5 h before adding to starch solution. The mixture is stirred till a gelatinized state achieved. The temperature fixed at $80 \text{ }^\circ\text{C}$ for 3 h. The obtained powder is dried at $60 \text{ }^\circ\text{C}$ for 24 h and milled. The final product calcined at $600 \text{ }^\circ\text{C}/2 \text{ h}$ with a heating rate $10 \text{ }^\circ\text{C}/\text{min}$.

Preparation of nZnO/Chitosan nanocomposite (nZnOCS nanocomposite)

1:1 nanocomposite is obtained by mixing 2 g of the calcined nZnO with 10 mL of ethanol, 20 mL of deionized water and 1 mL of 1 molL^{-1} HCl. The mixture stirred for 30 min. then added drop wisely to the prepared chitosan solution (0.5 g of chitosan was dissolved in 100 mL of 2% acetic acid). The solution was put in sonicator bath for 30 min. The composite is stirred for a day. This nanocomposite was left in open air for evaporating H_2O , followed by drying at $60 \text{ }^\circ\text{C}$ till constant mass.

Instruments

The homogeneity of the prepared composite is achieved by Ultrasonic Cole-Parmer instrument company version hills, Illinois 60061, USA. The identification of the present active functional groups of the composite assisted through Fourier transform infrared (FT-IR) spectra type Thermo Nicolet Nexus FT-IR, Waltham, MA, and (USA). The morphology of the particles informed by scanning electron microscope combined with energy-dispersive X-ray spectroscopy and electron backscatter diffraction type SEM, FEI Quanta FEG-250, and EDX. The nano character of the composite confirmed by transmission electron micrograph image, TEM, type JEM2100, Jeol.s.b, and (Japan). The phase structure studied using X-ray diffraction (XRD) type Philips X'PERT multipurpose X-ray diffractometer with copper emission lines. The thermal stability of the samples studied by Perkin Elmer TGA6 instrument. The sample was heated from 298 to 973 K at a heating rate of 283 K/min under nitrogen atmosphere with a flow rate of 20 ml/min. Particle size of the prepared samples determined using Zetasizer Nano-Zs, MALVERN (UK). Pore size distribution and corresponding porosity of the prepared powders investigated applying mercury intrusion porosimetry technique with the aid of Pore-sizer chromatech 9320 (USA).

The concentration of Cs(I) and/or Sr(II) were measured by an atomic absorption spectrophotometer (Buck Scientific, VGP 210).

Sorption studies

Batch sorption studies of the Cs(I) and Sr(II) onto nZnOCS nanocomposite. The variation in sorption parameters such as pH (1–9), metal ion concentration range (50–350 mgL⁻¹) temperatures (298, 313 and 333 K) and contact time (5–120 min) is checked to get the optimum condition for sorption.

Sorption experiments were conducted by batch techniques, by contact a certain weight of prepared samples (0.01 g) with 10 mL of the initial metal ion concentration of solution 200mgL⁻¹.

Sorbent and the sorbet solution were contacted in a batch-wise way and after sorption the samples separated from the solution by filtration. Metal concentrations in the test solution measured before and after sorption by atomic absorption measurements. The uptake percentage is calculated by Eq. (1).

$$\text{Uptake percent of Cs(I) or Sr(II) ions} = \left(\frac{C_0 - C_f}{C_0} \right) \times 100$$

Amount sorbed q (mgg⁻¹) calculated using Eq. (2):

$$q = (C_o - C_e) \frac{V}{m}$$

where q is the amount sorbed of the sorbent (mgg⁻¹). C_o , C_f and C_e are the initial, final, and equilibrium concentrations of the metal ions, respectively. V is the volume of solution (L) taken in (0.01 L), and m is the mass of the sorbent (g) taken in (0.01 g).

Saturation capacity

The saturation sorption capacity of nZnOCS nanocomposite towards of Cs(I) and Sr(II) ions was carried out using 0.05 g of nanocomposite with 10 ml of ions solution for 24 h. The sorbent was separated from the solution, and the concentrations of ions were determined. This step was repeated for several times using new 10 mL of metal ions solution until no further sorption of Cs(I) and Sr(II). The amount sorbed q_e (mgg⁻¹) was calculated for each equilibration using Eq. (2). The saturated sorption capacity of the nZnOCS nanocomposite towards Cs(I) and Sr(II) ions equal the total summation of successive amounts sorbed from Cs(I) and Sr(II) ions onto the composite at equilibrium. It could be determined applying Eq. (3).

$$\text{Saturation capacity} = \sum_{e=1}^n q_e \quad (3)$$

where n is the total number of times added new volumes.

Kinetics modelling studies

Various kinetic models were applied to investigate the mechanism of Cs(I) and Sr(II) retention on nZnOCS nanocomposite as pseudo 1st order and pseudo 2nd order.

The linear pseudo—1st order Eq. (4) is given by [24]:

$$\log(q_e - q_t) = \log q_e - \left(\frac{k_1}{2.303} \right) t$$

where q_e (mg g⁻¹), and q_t (mg g⁻¹), are the quantities of metal ion sorbed at equilibrium and at time t , respectively, and k_1 (min⁻¹), is the rate constant of the 1st order equation while the pseudo-2nd order linear Eq. (5) is expressed as [24]:

$$\frac{t}{q_t} = \frac{1}{k_2 q_e^2} + \frac{1}{q_e} t$$

where k_2 is a rate constant of the pseudo 2nd order model (g mg⁻¹ min⁻¹).

Elovich equation is applied for chemisorption kinetics. It is often evaluated for heterogeneous surfaces [25] and devised as in Eq. (6):

$$q_t = \frac{1}{\beta} \ln(\alpha\beta) + \frac{1}{\beta} \ln t$$

where α and β are the Elovich constants. α (mg g⁻¹ min⁻¹) represents initial sorption rate and β expressed desorption constant (g mg⁻¹) during any experiment related to the extent of surface coverage and also to the activation energy involved in chemisorption.

Intra-particle mass transfer diffusion rate constant (mgg⁻¹ min^{-0.5}) studied and described by the Eq. (7) [26].

$$q_t = K_{id} t^{0.5} + C$$

where k_{id} is the intra-particle diffusion rate constant (mgg⁻¹ min^{-0.5}) and C is the intercept, which can be calculated from the slope and intercept of the linear plots of q_t versus $t^{0.5}$, respectively.

Isotherm modeling studies

The isotherm models of the sorption reaction were analyzed in terms of Langmuir, Freundlich, Temkin.

The linear form of the Langmuir model can be expressed as the following Eq. (8) [27]:

$$\frac{1}{q_e} = \frac{1}{Q} + \frac{1}{bQ} \left(\frac{1}{C_e} \right)$$

where Q is the monolayer sorption capacity (mg g^{-1}), b is the constant related to the free energy of sorption ($b \propto e^{-\Delta G/RT}$) and C_e is the equilibrium metal ion concentration.

Using Langmuir equilibrium parameter, the favourability of the isotherm can be recognized by applying Eq. (9) and determined the value of R_L [5],

$$R_L = \frac{1}{1 + bC_o}$$

C_o is the initial metal ion concentration. The value of R_L gives an indication that the isotherm type is linear ($R_L = 1$), irreversible ($R_L = 0$), unfavourable ($R_L > 1$) or favourable ($0 < R_L < 1$).

The Gibbs free energy of sorption, ΔG (kJmol^{-1}) can also be evaluated from the parameter b according to the expression (10, 11) [28]:

$$K_e^o = b \times 1000 \times M \cdot \text{wt of adsorbate} \times \frac{[\text{Adsorbate}]^o}{\gamma} \quad (10)$$

$$\Delta G = -RT \ln K_e^o$$

where R is universal gas constant $8.314 \text{ J mol}^{-1} \text{ K}^{-1}$, and T is absolute temperature.

The values of other thermodynamic parameters such as ΔH^o (kJmol^{-1}) and ΔS^o ($\text{J mol}^{-1} \text{ K}^{-1}$) have been calculated using the following Eq. (12):

$$\ln K_e^o = \frac{\Delta S^o}{R} - \frac{\Delta H^o}{RT}$$

The relation between $\ln K_e^o$ and $1/T$ was plotted and give a straight line from the slope and the intercept of this line; the value of ΔH^o and ΔS^o has been estimated.

Also, the linear form of the Freundlich model can be expressed in Eq. (13) as the following [27]

$$\log q_e = \log K_f + \frac{1}{n} \log C_e$$

where K_f is the Freundlich sorption capacity coefficient ($\text{mg}^{1-1/n} \text{ L}^{1/n} \text{ g}^{-1}$), $1/n$ is the sorption intensity.

Temkin isotherm model assumes that the sorption heat of all molecules decreases linearly with the increase in coverage of the sorbent surface and that sorption is characterized by a uniform distribution of binding energies, up to maximum binding energy. The Temkin isotherm can be described by Eq. (14) [29].

$$q_e = \frac{RT}{b_T} \ln(A_T C_e) \quad (14)$$

where A_T is the equilibrium binding constant (L mol^{-1}) corresponding to the maximum binding energy, b_T is related to the sorption heat, R is the universal gas constant ($8.314 \text{ J K}^{-1} \text{ mol}^{-1}$) and T is the temperature (K). Temkin isotherm model takes into account the effects of indirect sorbent/sorbate interactions on the sorption process; it is also assumed that the heat of sorption of all molecules in the layer decreases linearly as a result of increased surface coverage.

Desorption studies

The desorption of studied ions was carried out by mixing the loaded material with 20 mL of eluents in 100 mL glass bottles and shaken at 180 rpm. The eluents HNO_3 , and HCl of various concentrations 0.1 molL^{-1} , 0.3 molL^{-1} and 0.5 molL^{-1} were used. The desorption percentage (%) was determined using the following Eq. (15):

$$\%D = \frac{C_d}{C_s} \times 100$$

where: C_s is the concentration of studied metal ions in solid phase. and C_d (mgL^{-1}) is the concentration of studied metal ions in aqueous phase.

Results and discussion

Characterization of the prepared materials

FT-IR analysis

The characteristic functional groups in the samples are already achieved by FT-IR analysis. Figure 1a a band at 3300 cm^{-1} is assigned to the O–H stretching mode of

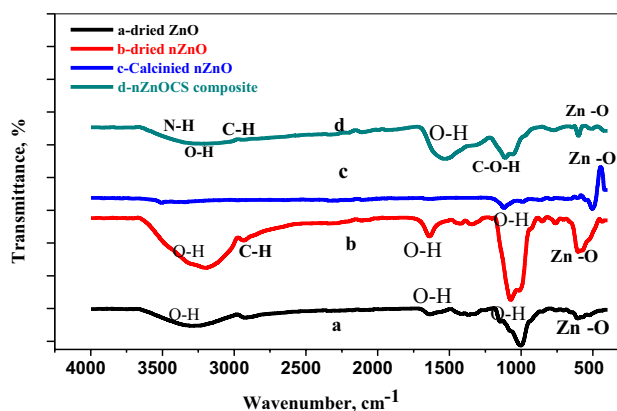


Fig. 1 FTIR of a dried ZnO b dried nZnO c calcined nZnO d nZnOCS nanocomposite C–O–H

hydroxyl group. The spectrum of ZnO (a) shows a characteristic absorption band at 533 cm^{-1} due to stretching of Zn–O. The small peak at 1003 cm^{-1} is assigned to normal polymeric O–H stretching vibration of H_2O in ZnO lattice [30]. A small broad peak at 1637 cm^{-1} is ascribed to the O–H bending mode due to hygroscopic adsorbed water.

The FTIR spectrum of the synthesized ZnO nanoparticles (nZnO) is displayed in Fig. 1b. The broad peak at 3200 cm^{-1} and the peak at 1638 cm^{-1} are assigned to the normal polymeric O–H stretching vibration of H_2O in ZnO lattice. The Zn–O maximum stretching vibration is split into two maxima, one at 603 , and 600 cm^{-1} [31]. The peak at 2932 cm^{-1} attributed to stretching vibration of the C–H for the starch matrix. 1421 cm^{-1} is assigned to C–O absorption band.

After calcinations, Fig. 1c, all O–H, C–H, C–O absorption bands disappear. A band at 1120 cm^{-1} is due to C–O while that for Zn–O appears at 504 cm^{-1} .

A characteristic broad peak for nZnOCS composite, Fig. 1d, at 3227 cm^{-1} corresponds to the overlap of stretching vibration of –NH and –OH groups. The absorption peaks of Chitosan at 1526 cm^{-1} related to amide group. Also, the absorption band at 1111 cm^{-1} is ascribed to bending vibration of C–O–H stretching group. There are new absorption peaks at 659 cm^{-1} and 465 cm^{-1} which are due to the attachment of amide group and stretching mode of ZnO [18].

The difference in shifting in the absorption band of Zn–O in ZnO, nZnO, calcined ZnO and nZnOCS attributed to the difference in the preparation constituents of the samples. In case of dried nZnO, Zn–O formed in starch host to stabilize nanoparticles. In calcined ZnO, the starch burns causes shifting of Zn–O from 603 to 504 cm^{-1} . For nZnOCS nanocomposite, Zn–O belongs to chitosan interaction and a big shift for Zn–O to 465 cm^{-1} .

Surface morphology

Figure 2 clarifies the particle size distribution of ZnO and nZnO particles. The nano character appears in nZnO as a result of using starch stabilizer. 98.3% of the particle size of nZnO is less than 100 nm as starch matrix prevents ZnO–NPs from undergoing spontaneous growth and aggregation [16]. However, ZnO which is synthesized without adding starch has a greater particle size ranges from 530 to 825 nm .

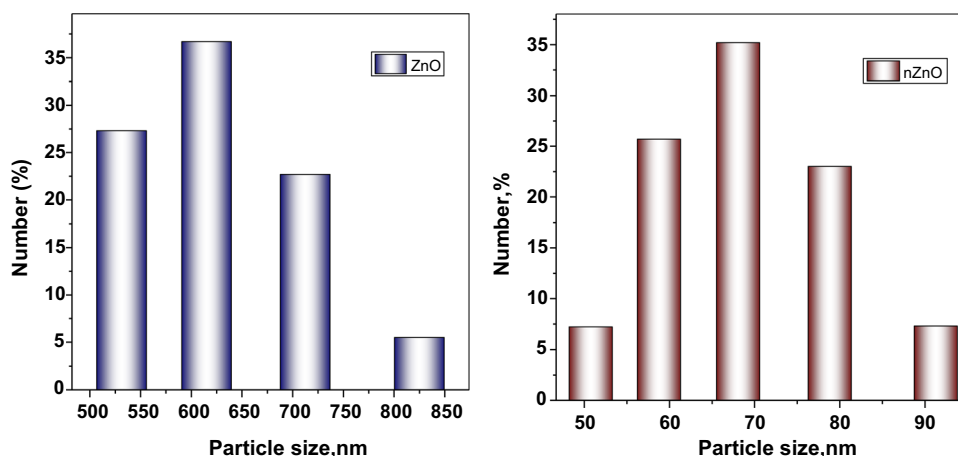
SEM of ZnO is shown in Fig. 3a. The particles are agglomerated. And the size is not in nanoscale and not separated. So, it concludes that zinc oxide prepared by hydrolysis of zinc nitrates without using starch as a matrix does not give a good surface morphology compared to that using starch as stabilizer.

TEM particle distribution result in Fig. 3b, c also confirmed the nano size of nZnO sample. The particle shape seems to be homogeneous and near hexagonal or nanosphere. Agglomeration of the particles appears and the particle size range between 11.54 and 13.67 nm . In case of nZnOCS composite in Fig. 3d, e the nano particles of nZnO adsorb onto the surface of chitosan with uniform distribution with the average particle size of 35 nm . The agglomeration of nZnO particles increases on the surface of chitosan [32].

X-Ray diffraction

The XRD of the prepared nano zinc oxide in Fig. 4. For dried nZnO in Fig. 4a amorphous structure is predominate with a characteristic low crystalline peak at 15° related to starch. After calcinations at 600°C , the starch burned and the crystalline peaks of wurtzite structure appeared at 31.06° , 34.2° and 36.02° (PDF Card: 00-036-1451) as shown in Fig. 4b. In Fig. 4c, the increase of the amorphous regions

Fig. 2 Particle size distribution of ZnO and nZnO samples (in dist. H_2O dispersed medium)



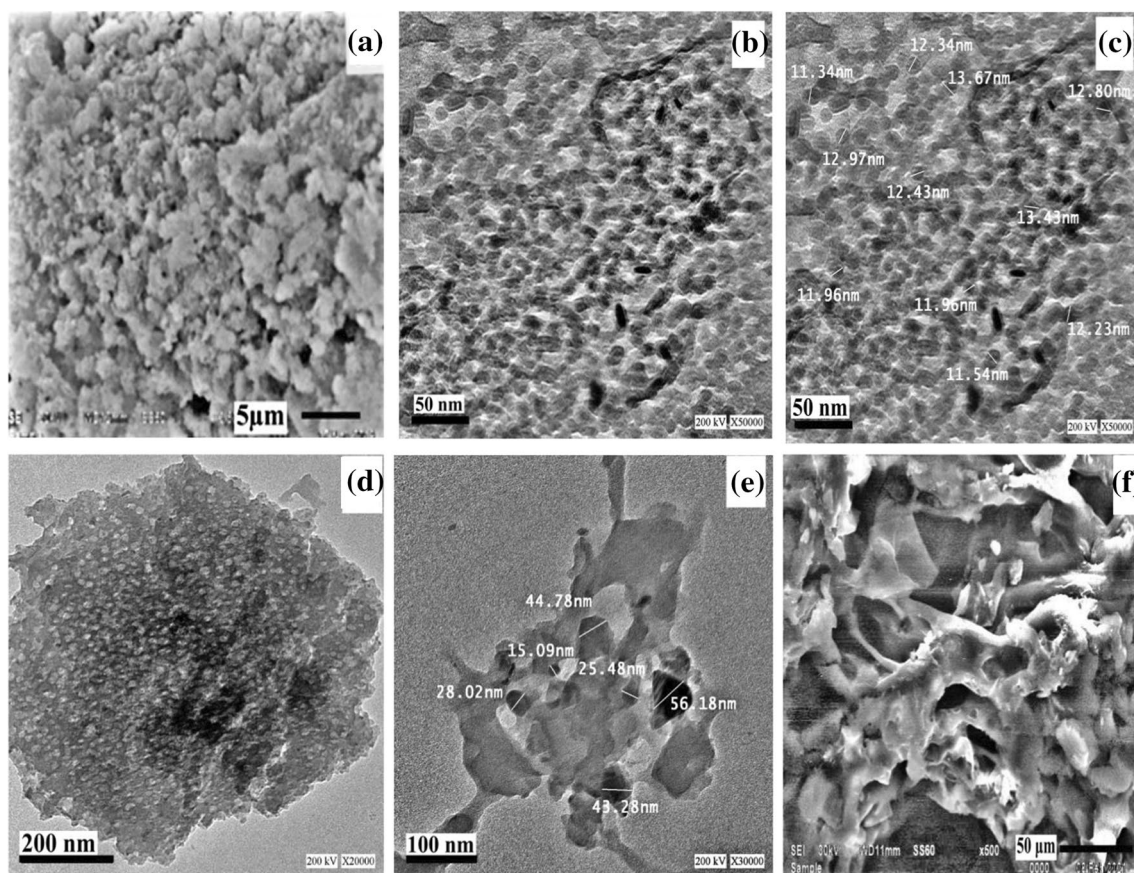


Fig. 3 a, f SEM of ZnO, nZnO b, c TEM of nZnO and d, e TEM of nZnOCS nanocomposite

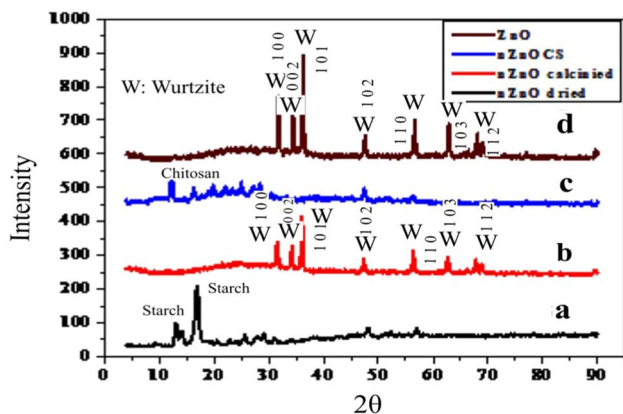


Fig. 4 XRD a dried nZnO b calcined nZnO and c nZnOCS nanocomposite d ZnO

in nZnOCS nanocomposites due to the interaction between the CS matrix and ZnO NPs and decreasing of water content [33]. Figure 4d depict ZnO crystal Wurtzite structure resembles nZnO crystal structure. But the peak for nZnO is more broad indicate the small size of the particles than ZnO [34].

Thermal analysis

Figure 5 shows the thermal stability of the prepared samples. ZnO shows great thermal stability and about 3.91% weight loss with two exothermic peaks at temperatures ranges 300–500 °C attributed to combustion of organic impurities.

In case of dried nano zinc oxide stabilized with starch (nZnO) has a low thermal stability reaches to 40% and the weight loss occurs in two stages. The first stage at 116 °C, 7.74% weight loss accompanied with endothermic peak due to desorption of physically sorbed water. The second stage with weight loss 52.3% starts from 244 °C till 600 °C with two exothermic peaks due to rate of degradation of starch into volatile combustible products [35].

For nZnOCS nanocomposite, from room temperature to 285 °C, a 14.73% weight loss related to the water evaporation and in the temperature more than 300 °C. Two endothermic peaks at temperatures below 300 °C while at temperature above 300 °C. A broad exothermic peak with ~47% weight loss due degradation of the CS.

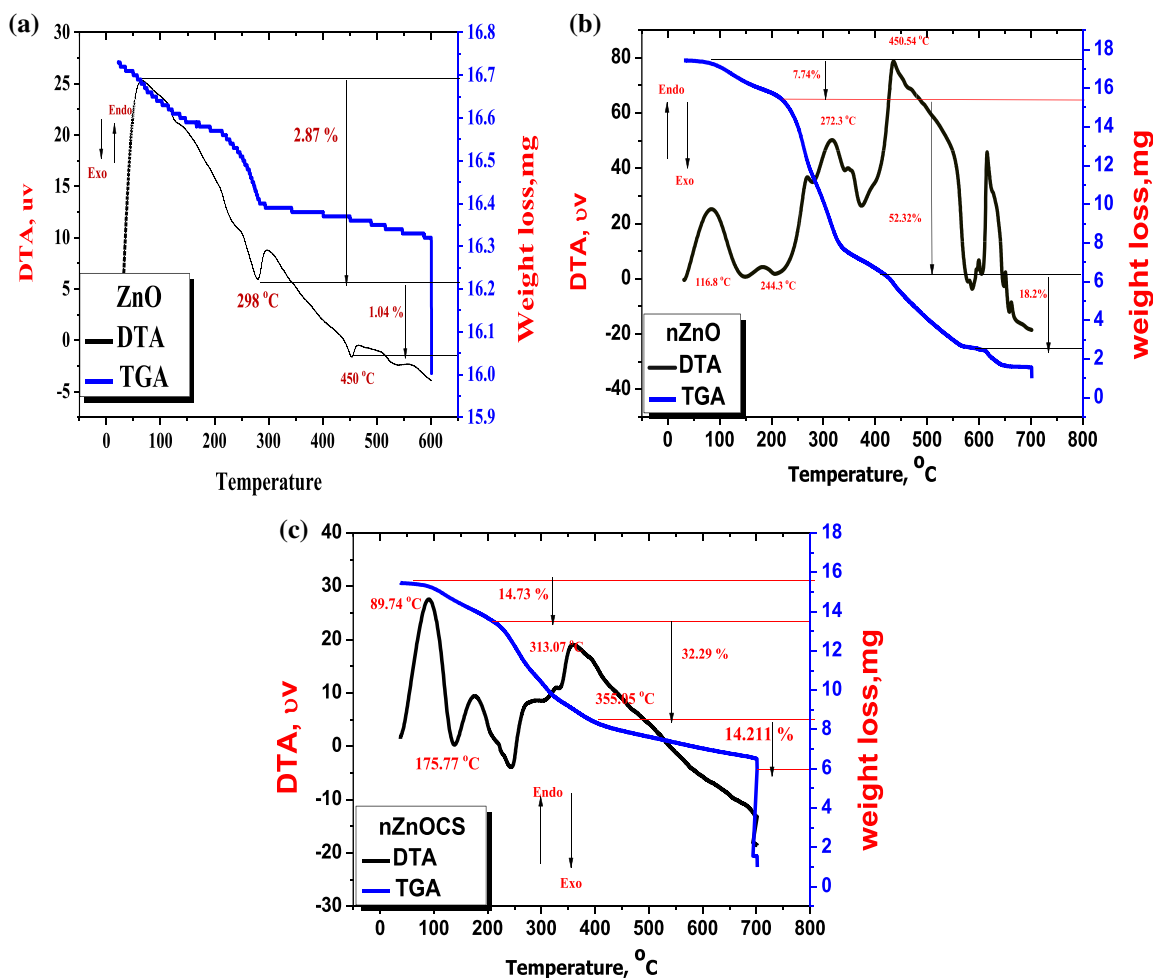


Fig. 5 DTA-TGA of a ZnO- calcined, b nZnO and c nZnOCS nanocomposite

Zero point charge (pHZPC)

Zero point charge (pH_{PZC}) is defined as the value of pH at which the charge of the surface of the composite is zero. At pH below this value the charge of the surface is positive and above this value the charge of the surface is negative.

The pH_{PZC} was determined using batch technique, the various glass bottles containing 20 mL of 0.1 molL^{-1} NaCl solution and 0.01 g of the ZnO, nZnO and nZnOCS nanocomposite. The solutions shaken at 25°C , the final pH was measured after 24 h. The pH_{PZC} was noted at the pH where the final pH equals the initial pH [36].

Figure 6 represents determination of zero point charge of ZnO, nZnO and nZnOCS nanocomposite. pH_{ZPC} of ZnO, nZnO are higher than 8 while for nZnOCS is less than 7 (nearly 6.8). Therefore, the surface charge of the composite may become positively or negatively charged depending on the pH value of the solution as follows:

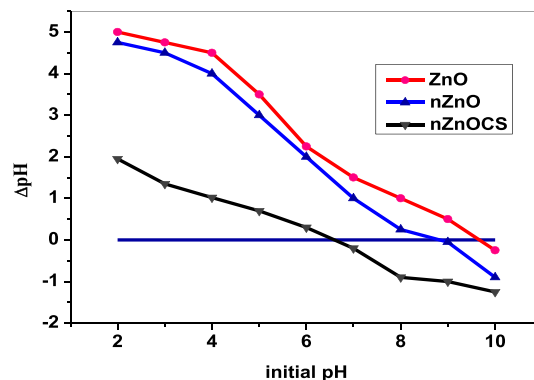


Fig. 6 Determination of pH_{ZPC} of ZnO, nZnO and nZnOCS (0.01 g in 20 mL of 0.1 molL^{-1} NaCl)

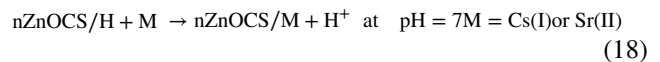


Sorption studies

Effect of pH

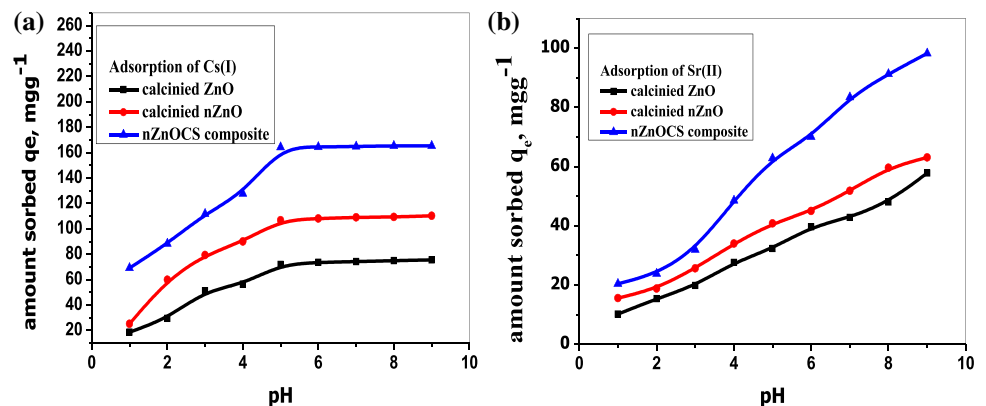
Studying the effect of pH on the sorption process is an important parameter owing to the speciation and/or solubility of metal ions depend on the pH of the solution. Different experiments were performed in the pH values from 1 to 9 (Fig. 7) to determine the optimum pH values. The sorbed amount q_e was found to increase with the increase pH owing to the increase of the electrostatic attraction forces between metal ions M and nZnOCS nanocomposite. i.e., at lower pH values, there is an excess of protons on composites

surface that resulting in an increase in the competition for sorption between protons and Cs(I) and Sr(II) ions. The amount sorbed of Cs(I) is nearly not changed by increase in pH above 5. However, in case of Sr(II), the sorbed amount increases as the pH increase. Figure 8 shows the speciation of Cs(I) and Sr(II) ions that carried out using Hydra/Medusa chemical equilibrium software [37] at initial metal ions concentration 200 mg L^{-1} , room temperature and different pH values (1–12). Cs(I) and Sr(II) are predominant species in pH range 1–10. The increase of Sr sorption in pH 7–10 may be due to the formation of colloids of strontium which adhered to the sorbent surface [38]. So, pH 7 was chosen for further sorption experiments. The mechanism of sorption reaction is given by Eq. (18).

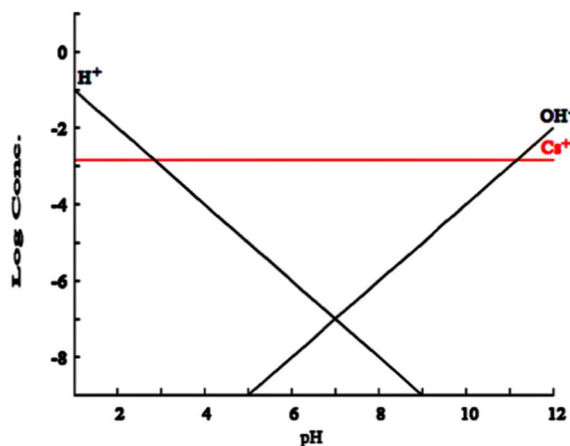


The sorption amount for Cs(I) is 74.2, 109 and 164.89 mg g^{-1} onto calcined ZnO, calcined nZnO and

Fig. 7 Adsorbed amount of **a** Cs(I) and **b** Sr(II) metal ions onto calcined ZnO, calcined nZnO and nZnOCS nanocomposite at different pH [$C_0 = 200 \text{ mg L}^{-1}$, $v/m = 1 \text{ L g}^{-1}$, Temperature = 298 K, Time = 24 h]

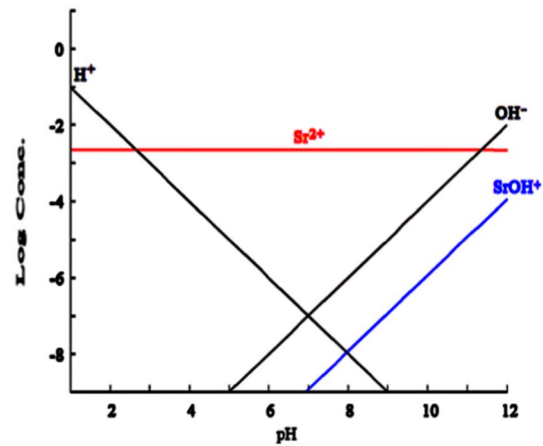


$[\text{Cs}^+]_{\text{TOT}} = 1.47 \text{ mM}$



(a)

$[\text{Sr}^{2+}]_{\text{TOT}} = 2.28 \text{ mM}$



(b)

Fig. 8 Speciation diagrams of Cs(I) and Sr(II) at different pH at 25 °C

nZnOCS nanocomposite, respectively. While for Sr(II) is 42.8, 51.8 and 83.39 mg g⁻¹, respectively.

Effect of contact time & temperature

Figure 9 depicted the relation between the sorbed amount of Cs(I), Sr(II) onto nZnOCS nanocomposite and the contact time at different working temperatures; 298, 313, and 333 K. The effect of temperature investigated with respect to time (5–120 min). The equilibrium time of the sorption process reached at nearly 60 min. The sorption reaction rate of the selected sorbed metal ions is very rapid at the early contact times and then becomes very slow near the equilibrium this is due to the availability of active sites on the surface of the sorbent at the early contact and increase of the occupied sites near the equilibrium. The sorbed amount increased by increasing time till the equilibrium. Figure 9 indicated that the sorption process is temperature-dependent and the sorbed amount increased as the temperature increased giving an expectation for endothermic nature of the process.

Fig. 9 Effect of contact time on the adsorbed amount of Cs(I) and Sr(II) onto nZnOCS nanocomposite at different temperatures [$C_o = 200 \text{ mg L}^{-1}$, $v/m = 1 \text{ L g}^{-1}$, $\text{pH} = 7$]

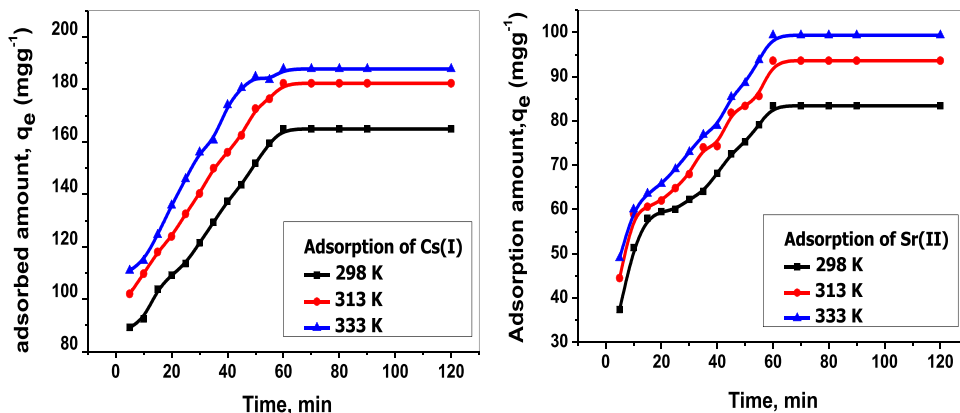
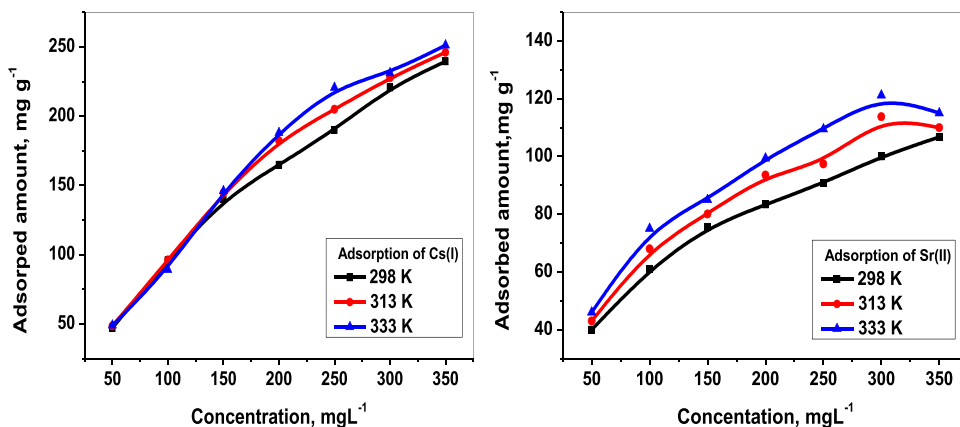


Fig. 10 Effect of initial concentration of Cs (I) or Sr (II) onto nZnOCS nanocomposite at different temperatures [Eq. Time = 60 min, $v/m = 1 \text{ L g}^{-1}$, $\text{pH} = 7$]



Effect of metal ion concentration

Figure 10 shows the plots between the amount of Cs(I) and Sr(II) sorbed at equilibrium q_e , onto nZnOCS nanocomposite and the initial metal ion concentrations C_o . The sorbed amount of Cs(I) or Sr(II) onto nZnOCS nanocomposite increases as the initial concentration of the sorbed metal ion increase. The sorbed amount increases by increasing temperature indicating that the sorption of metal ions by sorbent may involve not only physical sorption but also chemical sorption [39].

Saturation capacity

Saturation capacities of nZnOCS nanocomposite towards Cs(I) and Sr(II) were studied. The values of saturation capacities were 312.12 and 241.35 mg g⁻¹ for Cs(I) and Sr(II), respectively.

Table 1 Fitting results of kinetic data using pseudo-1st order model, pseudo-2nd order model, and Elvoich model

Metal ion	Temperature, K	Pseudo-first-order	$q_{e(\text{exp.})}$	Pseudo-second-order	Elvoich
Cs(I)	298 K	$q_{e(\text{cal.})} = 131.3711 \pm 8.1$ $K_1 = 0.0454 \pm 0.0031$ $R_2 = 0.85$	164.8986 ± 7.1	$q_{e(\text{cal.})} = 185.87 \pm 9.1$ $K_2 = 0.0212 \pm 0.0005$ $R_2 = 0.96$	$\alpha = 64.51 \pm 1.9$ $\beta = 0.0315 \pm 0.0011$
	313 K	$q_{e(\text{cal.})} = 139.6496 \pm 8.6$ $K_1 = 0.0485 \pm 0.0053$ $R_2 = 0.89$	182.2822 ± 8.6	$q_{e(\text{cal.})} = 204.082 \pm 9.8$ $K_2 = 0.0216 \pm 0.0006$ $R_2 = 0.97$	$\alpha = 88.3989 \pm 2.4$ $\beta = 0.02941 \pm 0.0051$ $R_2 = 0.9$
	333 K	$q_{e(\text{cal.})} = 156.823 \pm 8.3$ $K_1 = 0.0624 \pm 0.0061$ $R_2 = 0.93$	187.7979 ± 8.9	$q_{e(\text{cal.})} = 212.766 \pm 9.5$ $K_2 = 0.0225 \pm 0.0004$ $R_2 = 0.99$	$\alpha = 85.5233 \pm 4.1$ $\beta = 0.02602 \pm 0.0062$ $R_2 = 0.9$
Sr(II)	298 K	$q_{e(\text{cal.})} = 54.954 \pm 3.5$ $K_1 = 0.0381 \pm 0.0025$ $R_2 = 0.88$	83.39588 ± 4.5	$q_{e(\text{cal.})} = 90.498 \pm 2.9$ $K_2 = 0.0329 \pm 0.0024$ $R_2 = 0.97$	$\alpha = 32.381 \pm 2.3$ $\beta = 0.062 \pm 0.0043$ $R_2 = 0.93$
	313 K	$q_{e(\text{cal.})} = 65.463 \pm 3.7$ $K_1 = 0.03867 \pm 0.0022$ $R_2 = 0.86$	93.58914 ± 4.7	$q_{e(\text{cal.})} = 101.01 \pm 3.2$ $K_2 = 0.031 \pm 0.0027$ $R_2 = 0.97$	$\alpha = 41.416 \pm 3.4$ $\beta = 0.0575 \pm 0.0063$ $R_2 = 0.9$
	333 K	$q_{e(\text{cal.})} = 67.78 \pm 3.2$ $K_1 = 0.0368 \pm 0.0031$ $R_2 = 0.89$	99.35091 ± 5.1	$q_{e(\text{cal.})} = 108.342 \pm 3.6$ $K_2 = 0.0289 \pm 0.0021$ $R_2 = 0.96$	$\alpha = 39.974 \pm 3.2$ $\beta = 0.054 \pm 0.0054$ $R_2 = 0.89$

Kinetic modeling

Table 1 and Fig. 11 show the fitted diagrams based on the pseudo-1st-order model, pseudo-2nd-order model, Elvoich model and intra particle diffusion model at three different temperatures.

As shown in Fig. 11 and Table 1, the pseudo-2nd-order model has a better correlation coefficient ($R^2 \geq 0.96$) than that of the pseudo-1st-order model ($R^2 \geq 0.85$). Furthermore, the values of calculated capacity of the sorbed metal ions at equilibrium $q_{e(\text{cal.})}$ are nearly in identity with the values of the experimental data $q_{e(\text{exp.})}$. This clearly suggests that the sorption kinetics of metal ions is accurately supported with the pseudo-2nd-order and the sorption process is controlled by chemisorptions process [40, 41].

It can be concluded that the three kinetics models are found to be suitable for fitting the present sorption kinetics data in the following subsequent order: Pseudo 2nd order > Elovich > pseudo 1st order.

The intra particle diffusion model represented by the relation between q_t and $t^{0.5}$ of the sorption of metal ions at various temperatures is given in Fig. 11. The intercept which is the thickness of the surface gave information about contribution of the surface sorption in the rate-determining step. The larger the intercept, the greater is its contribution. It is obvious that the intra-particle diffusion kinetic model for the sorption process of the two metal ions occurred through three stages. The first stage describes the diffusion of the metal ions from the solution to the surface of the nZnOCS nanocomposite (from 1 to 20 min). The second stage (from

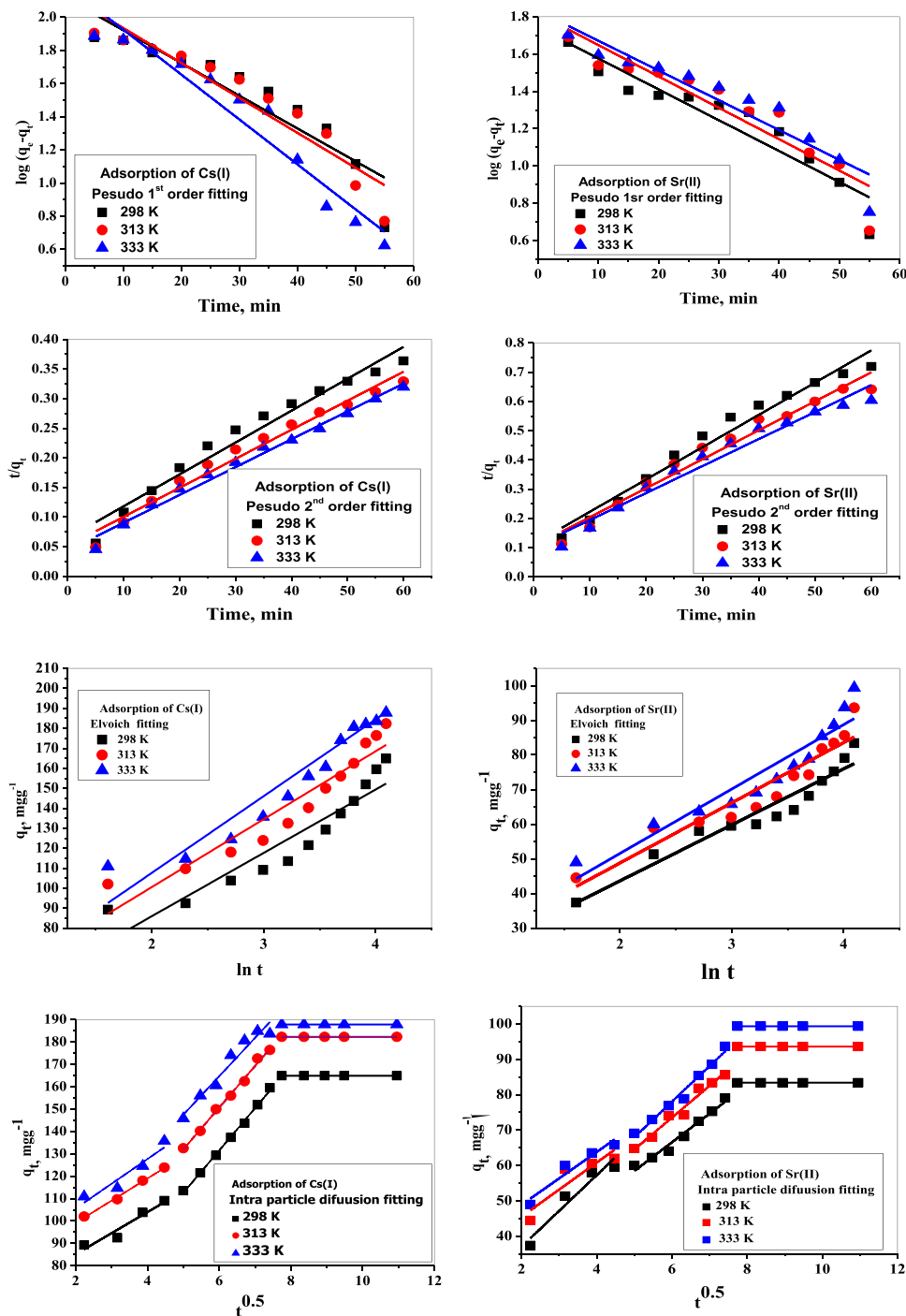
25 to 55 min) designs the gradual sorption on the surface of the nZnOCS nanocomposite, which may be the rate-limiting step. The third one (from 60 to 120 min) is the equilibrium saturation. The multi-diffusion step is the main factor in the control of the sorption mechanism, that encompasses both film and intra-particle diffusion. Table 2 shows the parameters obtained from the second part of the linear plot.

Isotherm modeling

Langmuir, Freundlich and Temkin Isotherm were applied for Cs(I) and Sr(II) sorption onto nZnOCS nanocomposite at different temperatures and represented in Fig. 12. The calculated parameters according to Eqs. (8, 9, 13 and 14) were given in Table 3. Maximum sorption capacity for Langmuir was found 253.806, 116.1 mg g⁻¹ for Cs(I) and Sr(II), respectively. The maximum sorption capacity increase with temperature confirming the endothermic nature of the sorption process. As noted from Table 3, the value of R_L is ($0 < R_L < 1$) gives an indication that the sorption of Cs(I) and Sr(II) is favourable onto nZnOCS nanocomposite.

Freundlich isotherm constants k_f and n were determined from the intercept and slope of a plot of $\log q_e$ versus $\log C_e$. The parameters for Langmuir and Freundlich isotherm fits (Table 3) yielded isotherms that are in a good conformity of detected correlation coefficient for Sr(II) ($R^2 \geq 0.98$) but in case of Cs(I) is better described by Langmuir where $R^2 \geq 0.978$ higher than that of Freundlich ($R^2 \geq 0.79$). This may be attributed to difference in ionic size between Cs(I) and Sr(II), and the pore size consideration of nZnOCS

Fig. 11 Kinetic modelling fitting of Cs (I) or Sr (II) sorption onto nZnOCS nanocomposite at different temperatures [$C_0 = 200 \text{ mg L}^{-1}$, $v/m = 1 \text{ L g}^{-1}$, $\text{pH} = 7$]



nanocomposite. K_f was raised by temperature, so the sorption process was endothermic [42].

The constants of A_T and b_T for Temkin fitting determined from the slope and intercept of the plot of q_e against $\ln C_e$. These constants correlated to the sorption capacity and intensity of sorption. R^2 , correlation coefficient value is close to unity indicating the sorption mechanism which is governed by chemisorption process.

Desorption studies

The desorption studies were carried out by washing loaded material with various desorbing agents such as HNO_3 , and HCl with different concentrations 0.1 mol L^{-1} , 0.3 mol L^{-1} and 0.5 mol L^{-1} . As the concentration of the desorbing agents increase, the desorption efficiency increases. HNO_3 is more preferred as desorbing agent than HCl as the

Table 2 Diffusion models parameters for sorption of Cs(I) and Sr(II) metal ions onto nZnOCS nanocomposite at different temperatures

Sorbent	Temperature, K	Intra-particle diffusion model			
		Time range, min	Kid, g mg ⁻¹ min ⁻¹	C	R ²
nZnOCS	Cs(I)—298	5–20	9.40±1.814	66.32±6.413	0.9
		25–55	18.93±0.45	17.88±2.82	0.996
		60–120	–	164.8986	–
	Sr(II)—298	5–20	10.112±1.96	16.81±6.93	0.90
		25–55	8.10±0.594	17.918±3.75	0.97
		60–120	–	83.395	–
	Cs(I)—313	5–20	9.914±0.493	79.313±1.74	0.99
		25–55	18.61±0.6091	38.982±3.85	0.994
		60–120	–	182.22	–
Sr(II)—313	5–20	7.647±2.5166	30.255±8.89	0.73	
	25–55	9.00±0.708	19.49±4.48	0.97	
	60–120	–	93.58	–	
Cs(I)—333	5–20	11.048±2.42	83.469±8.56	0.868	
	25–55	17.17±1.766	61.62±11.17	0.94	
	60–120	–	197.79	–	
Sr(II)—333	1–25	7.46±1.454	33.93±5.141	0.89	
	30–50	10.049±0.651	17.73±4.11	0.98	
	60–100	–	99.35	–	

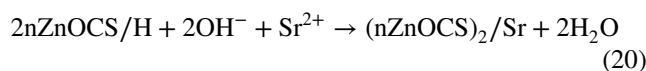
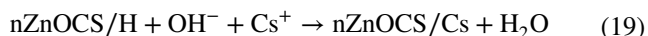
desorption efficiency using HNO₃ acid was found to be better than that using HCl acid at the same concentration. From the Fig. 13, HNO₃ acid (0.5 molL⁻¹) shows optimum desorption of Cs (I), and Sr (II), with desorption efficiency 83% and 99.3%, respectively.

Thermodynamic study

According to Eqs. (10–12), the values of ΔH° and ΔS° can be calculated from the slope and intercept of the plot of $\ln K_e^\circ$ against $1/T$ yields, respectively (Fig. 14). Results are shown in Table 4. The positive value of ΔH° indicates the endothermic nature of the sorption process and the positive value of ΔS° suggests the increase in randomness at the nanocomposite/solution interface during the sorption process. The negative value ΔG° indicates the sorption process is spontaneous. The increase in negative value of Gibbs free energy with temperature raising indicate a high degree of spontaneity of the process and an endothermic nature of the prepared sample.

Mechanism of the sorption reaction

Cs(I) and Sr(II) sorptions onto nZnOCS at pH 7 with initial concentration 200 mgL⁻¹ favoured cation sorption. A possible cationic sorption reaction can be expressed as:



Comparison with other sorbents

There are several sorbents used as sorbent for Cs(I) and Sr(II) from aqueous solution [43–48]. A comparison of the monolayer capacity, experimental adsorption capacity and maximum saturation capacity for Cs(I) and/or Sr(II) onto other sorbents with that sorbed onto nZnOCS nanocomposite is listed in Table 5. It is obvious from Table 5; nZnOCS nanocomposite is an efficient bio-sorbent for Cs(I) and Sr(II) ions from aqueous solutions.

Conclusion

1:1 ZnO/Chitosan nanocomposite successfully prepared by sol–gel method. ZnO is prepared using two different methods; hydrolysis of zinc nitrate by NaOH (ZnO) and hydrolysis of zinc nitrate in presence of starch as stabilizer (nZnO). The prepared samples calcined at 600 °C/2 h. nZnO shows a nanocharacter when examined by particle size distribution and TEM analysis. 1:1 nZnO: Chitosan nanocomposite successfully prepared by sol–gel method. Different analytical

Fig. 12 Isothermal modelling fitting of Cs(I) or Sr(II) sorption onto nZnOCS nanocomposite at different temperatures [Eq. Time = 60 min, v/m = 1Lg⁻¹, pH = 7]

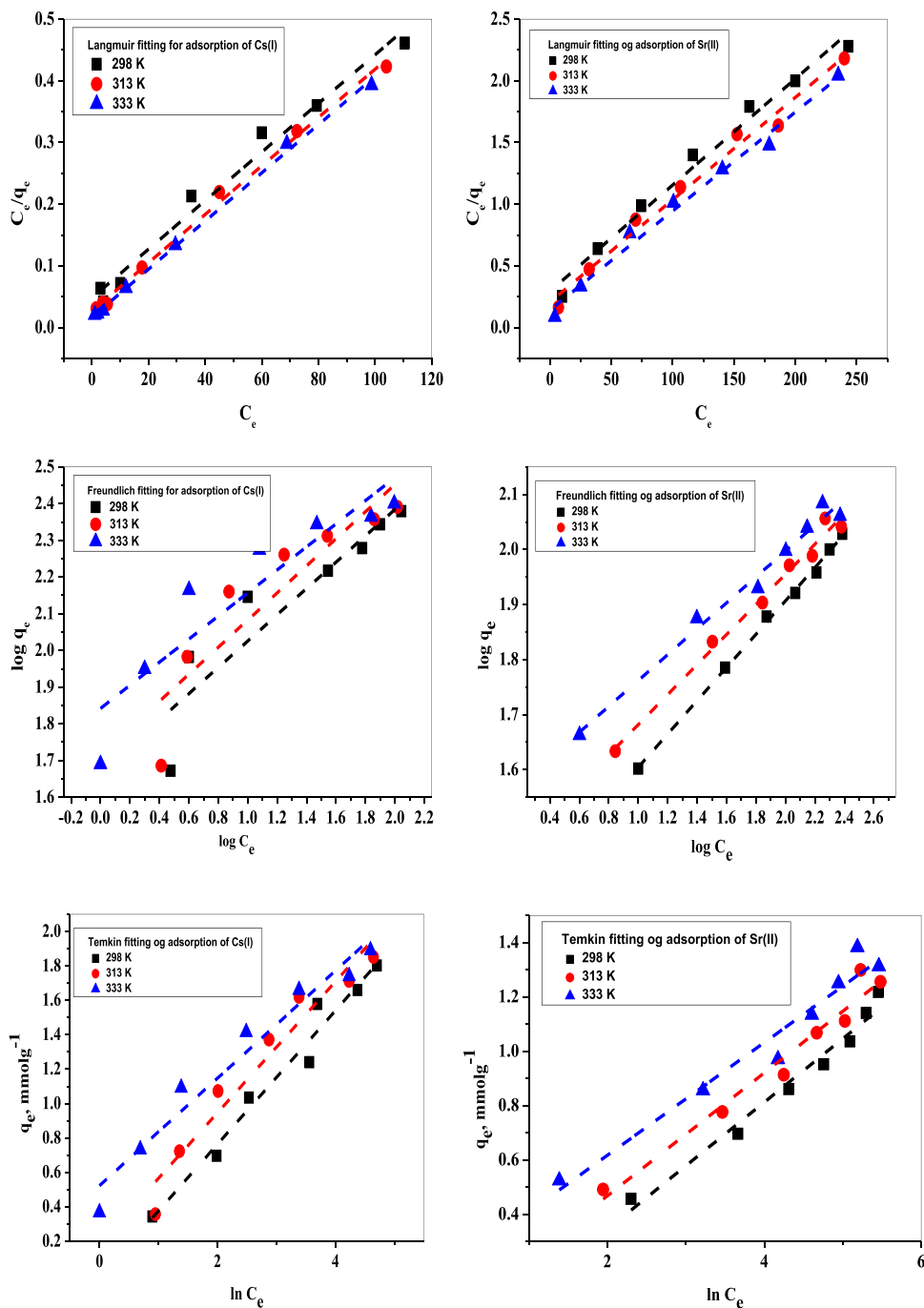


Table 3 Fitting results of isotherm for Langmuir, Freundlich and Temkin models

Metal ions	Temp., K	Freundlich isotherm model			Langmuir isotherm model				Temkin isotherm model		
		$K_f \text{ mg}^{1-1/n} \text{ L}^{1/n} \text{ g}^{-1}$	n	R^2	$Q \text{ (mgg}^{-1}\text{)}$	$b, \text{ Lg}^{-1}$	R_L	R^2	$A_T \text{ (L mol}^{-1}\text{)}$	$b_T \text{ (kJ mol}^{-1}\text{)}$	R^2
Cs(I)	298	45.70 ± 3.1	2.789	0.82	253.81 ± 6.6	0.0821 ± 0.001	0.057	0.978	0.968 ± 0.001	6.373 ± 0.9	0.97
	313	51.64 ± 3.5	2.707	0.79	255.10 ± 6.8	0.1475 ± 0.003	0.032	0.995	1.618 ± 0.002	6.811 ± 0.7	0.94
	333	69.510 ± 4.1	3.179	0.83	255.75 ± 6.4	0.2394 ± 0.005	0.020	0.997	5.3423 ± 0.03	8.858 ± 0.6	0.95
Sr(II)	298	3.908 ± 0.07	3.64	0.98	116.1 ± 4.5	0.0293 ± 0.002	0.146	0.98	0.5903 ± 0.0064	10.754 ± 1.1	0.97
	313	3.945 ± 0.08	3.39	0.98	120.48 ± 3.5	0.0403 ± 0.002	0.110	0.98	1.068 ± 0.0072	11.474 ± 1.2	0.96
	333	4.102 ± 0.09	3.33	0.975	124.53 ± 3.9	0.0571 ± 0.003	0.081	0.985	2.659 ± 0.0068	13.314 ± 1.3	0.95

Fig. 13 Desorption studies of Cs(I) and Sr(II) ions at 298 K from loaded material using **a** HNO₃ and **b** HCl at different concentrations [C_o of Cs(I) = 164.89 mgL⁻¹, C_o of Sr(II) = 83.39 mgL⁻¹, $v/m = 1\text{Lg}^{-1}$, time = 24 h]

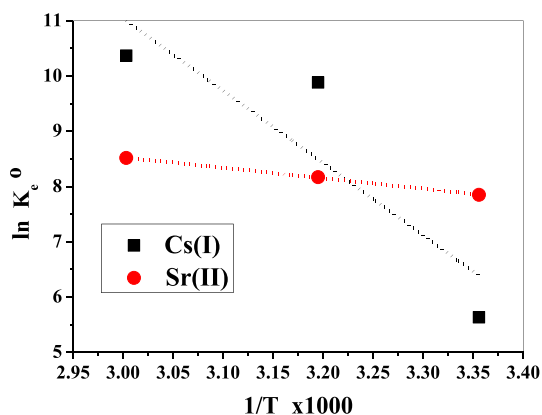
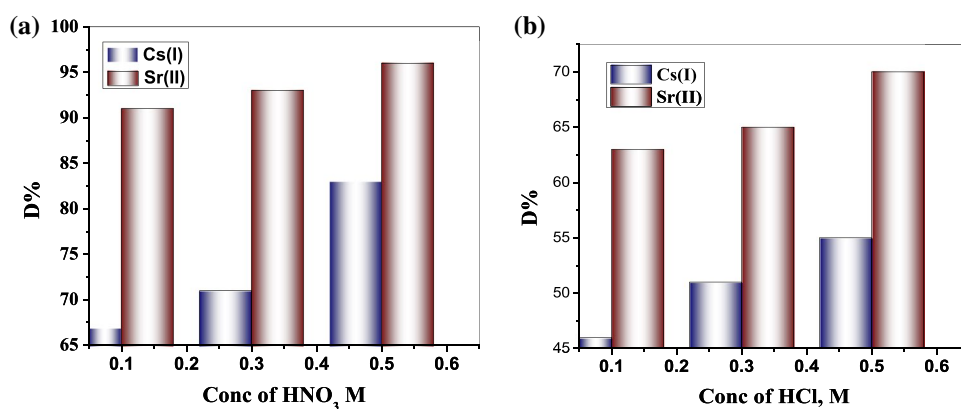


Fig. 14 A plot of $\ln K_c^\circ$ against $1000/T$ for Cs(I) and Sr(II) sorption onto nZnOCS [Eq. Time = 60 min, $v/m = 1\text{Lg}^{-1}$, pH = 7]

techniques like FTIR, XRD, DTA-TGA, and pore size analysis used for studying the physic-chemical properties. The prepared composite used as a sorbent for Cs(I) and Sr(II) from aqueous solution. The optimum pH for sorption reaction is 7. The sorption process carried out at three different temperatures 298 K, 313 K and 333 K. The sorption reaction is fast, and the reaction equilibrium attained after an hour. Pseudo 2nd order model is applicable with the sorption reaction mechanism. The sorption mechanism belongs to Langmuir model and the monolayer capacities of Cs(I) and Sr(II) at pH 7 at 298 K are 253.81 and 116.1 mgg⁻¹, respectively. Thermodynamic studies clarified that the sorption reaction is endothermic, and the process is spontaneous.

Table 4 Thermodynamic parameters for the sorption of Cs(I) and Sr(II) metal ions onto nZnOCS nanocomposite

Metal ions	ΔG° , kJ mol ⁻¹			ΔH° , kJ mol ⁻¹	ΔS° , J mol ⁻¹ K ⁻¹
	298 K	313 K	333 K		
Cs(I)	-15.84 ± 1.2	-22.113 ± 1.3	-30.474 ± 1.4	108.74 ± 1.1	418.06 ± 2.6
Sr(II)	-19.47 ± 0.7	-21.24 ± 0.8	-23.60 ± 1.9	15.705 ± 0.9	118.0255 ± 2.4

Table 5 Comparison of adsorption capacities of various materials for adsorption of Cs(I) and Sr(II) from aqueous solution

Adsorbent materials	Adsorption monolayer capacity		Experimental adsorption capacity		Maximum saturation capacity		References
	Cs(I)	Sr(II)	Cs(I)	Sr(II)	Cs(I)	Sr(II)	
Magnetic graphene oxide at pH = 4 and 293 K	9.259 mgg ⁻¹	14.70 mgg ⁻¹	NR	NR	NR	NR	[43]
Irradiated <i>Saccharomyces cerevisiae</i> pH = 5 for Sr (II) and Cs (I) at pH = 6 and 305 K	18.778 mgg ⁻¹	56.44 mgg ⁻¹	12.93 mgg ⁻¹	18.91 mgg ⁻¹	NR	NR	[44]
Zeolite	1.7848 mmol g ⁻¹	0.764 mmolg ⁻¹	NR	NR	NR	NR	[45]
Activated charcoal modified with Prussian blue nanoparticle at pH 6.5 at 298 K	36.1 mgg ⁻¹	9.26 mgg ⁻¹	18.52 mgg ⁻¹	14.17 mgg ⁻¹	67.9 mgg ⁻¹	29.6 mgg ⁻¹	[46]
Brewery's waste at pH = 4 and 303 K	0.076 mmolg ⁻¹	0.091 mmolg ⁻¹	NR	NR	NR	NR	[47]
BS at 298 K	948 mgg ⁻¹	441.6 mgg ⁻¹	519.4 mgg ⁻¹	632.5 mgg ⁻¹	NR	NR	[48]
nZnOCS nanocomposite at pH=7 and 298 K	253.81 mgg ⁻¹	116.1 mgg ⁻¹	164.89 mg g ⁻¹	83.39 mgg ⁻¹	312.12 mgg ⁻¹	241.35 mgg ⁻¹	This work

NR not reported

Author contributions All authors contributed to the study conception and design. Material preparation, data collection and analysis. All authors read and approved the final manuscript.

Declarations

Conflict of interest The authors declare that they have no conflict of interest.

References

- Al Attar L, Safia B, Ghani BA (2018) Uptake of ¹³⁷Cs and ⁸⁵Sr onto thermally treated forms of bentonite. *J Environ Radioact* 193–194:36–43
- Dakroury GA, Abo-Zahra SF, Hassan HS, Ali HEA (2020) Improvement of the sorption behavior of aluminum silicate composite toward ¹³⁴Cs and ⁶⁰Co radionuclides by non-living biomass of *Chlorella vulgaris*. *Environ Sci Pollut Res* 27(17):21109–21125. <https://doi.org/10.1007/s11356-020-08260-y>
- Ma F, Li Z, Zhao H, Geng Y, Zhou W, Li Q, Zhang L (2017) Potential application of graphene oxide membranes for removal of Cs(I) and Sr(II) from high level-liquid waste. *Sep Purif Technol* 188:523–529
- Synhaeve N, Stefani J, Tournlonias E, Dublineau I, Bertho JM (2011) Biokinetics of ⁹⁰Sr after chronic ingestion in a juvenile and adult mouse model. *Radiat Environ Biophys* 50:501–511
- Chegrouche S, Mellah A, Barkat M (2009) Removal of strontium from aqueous solutions by adsorption onto activated carbon: kinetic and thermodynamic studies. *Desalination* 235:306–318. <https://doi.org/10.1016/j.desal.2008.01.018>
- Ibrahim HA, Hassan HS, Mekhamer HS, Kenawy SH (2019) Diffusion and sorption of Cs⁺ and Sr²⁺ ions onto synthetic mullite powder. *J Radioanal Nucl Chem* 319:1–12
- Hu YM, Guo X, Chen C, Wang JL (2019) Algal sorbent derived from *Sargassum horneri* for adsorption of cesium and strontium ions: equilibrium, kinetics, and mass transfer. *Appl Microbiol Biotechnol* 103:2833–2843
- Wang JL, Chen C (2014) Chitosan-based biosorbents: modification and application for biosorption of heavy metals and radionuclides. *Bioresour Technol* 160:129–141
- Dakroury GA, Abo-Zahra SF, Hassan HS (2020) Utilization of olive pomace in nano MgO modification for sorption of Ni(II) and Cu(II) metal ions from aqueous solutions. *Arab J Chem* 13(8): 6510–6522, ISSN 1878-5352 <https://doi.org/10.1016/j.arabjc.2020.06.008>.
- Huang KS, Yang CH, Huang SL, Chen CY, Lu YY, Lin YS (2016) Recent advances in antimicrobial polymers: a mini-review. *Int J Mol Sci* 17(9):1578–1592
- Farzana MH, Meenakshi S (2015) Photocatalytic aptitude of titanium dioxide impregnated chitosan beads for the reduction of Cr(VI). *Int J Biol Macromol* 72:1265–1271
- Kandile NG, Mohamed HM, Mohamed MI (2015) New heterocycle modified chitosan adsorbent for metal ions (II) removal from aqueous systems. *Int J Biol Macromol* 72:110–116. <https://doi.org/10.1016/j.ijbiomac.2014.07.042>
- Xiaodong M, Zhang Z, Dai E, Guo H (2016) Improved multi-shot diffusion imaging using GRAPPA with a compact kernel. *NeuroImage* 138:88–99. <https://doi.org/10.1016/j.neuroimage.2016.05.079>
- Shahzad A, Miran W, Rasool K, Nawaz M, Jang J, Le LS (2017) Heavy metals removal by EDTA-functionalized chitosan graphene oxide nanocomposites. *RSC Adv* 7:9764–9771. <https://doi.org/10.1039/C6RA28406J>
- Zhang F, Chen X, Wu F, Ji Y (2016) High adsorption capability and selectivity of ZnO nanoparticles for dye removal. *Coll Surf A Physicochem Eng Asp* 509:474–483. <https://doi.org/10.1016/j.colsurfa.2016.09.059>
- Zak AK, Abd Majid WH, Mahmuodian MR, Majid D, Yousefi R (2013) Starch-stabilized synthesis of ZnO nanopowders at low temperature and optical properties study. *Adv Powder Technol* 24(3):618–624. <https://doi.org/10.1016/j.apt.2012.11.008>
- Rahman PM, Abdul Mujeeb VM, Muraliedharan K, Thomas SK (2018) Chitosan/nano ZnO composite films: Enhanced mechanical, antimicrobial and dielectric properties. *Arab J Chem* 11(1):120–127, ISSN 1878-5352 <https://doi.org/10.1016/j.arabjc.2016.09.008>
- Abdelhady MM (2012) Preparation and characterization of chitosan / zinc oxide nanoparticles for imparting antimicrobial and UV protection to cotton fabric. *Int J Carbohydr Chem* 2012:1–6. <https://doi.org/10.1155/2012/840591>

19. Al-Naamani L, Dobretsov S, Dutta J (2016) Chitosan-zinc oxide nanoparticle composite coating for active food packaging applications. *Innov Food Sci Emerg Technol* 38:231–237. <https://doi.org/10.1016/j.ifset.2016.10.010>
20. Zhong R, Zhong Q, Huo M, Yang B, Li H (2020) Preparation of biocompatible nano-ZnO/chitosan microspheres with multi-functions of antibacterial, UV-shielding and dye photodegradation. *Int J Biol Macromol* 146:939–945. <https://doi.org/10.1016/j.ijbiomac.2019.09.217>
21. Yusof NAA, Zain NM, Pauzi N (2019) Synthesis of ZnO nanoparticles with chitosan as stabilizing agent and their antibacterial properties against Gram-positive and Gram-negative bacteria. *Int J Biol Macromol* 124:1132–1136. <https://doi.org/10.1016/j.ijbiomac.2018.11.228>
22. Saad AHA, Azzam AM, El-Wakeel ST, Mostafa BB, Abd El-lati MB (2018) Removal of toxic metal ions from wastewater using ZnO@Chitosan core-shell nanocomposite. *Environ Nanotechnol Monit Manag* 9:67–75. <https://doi.org/10.1016/j.enmm.2017.12.004>
23. Mohan AC, Renjanadevi B (2016) Preparation of zinc oxide nanoparticles and its characterization using scanning electron microscopy (SEM) and X-Ray diffraction (XRD). *Procedia Technol* 24:761–766. <https://doi.org/10.1016/j.protcy.2016.05.078>
24. Lin J, Wang L (2009) Comparison between linear and non-linear forms of pseudo-first-order and pseudo-second-order adsorption kinetic models for the removal of methylene blue by activated carbon. *Front Environ Sci Eng China* 3:320–324. <https://doi.org/10.1007/s1783-009-0030-7>
25. Cheung CW, Porter JF, Mckay G (2000) Sorption kinetics for the removal of copper and zinc from effluents using bone char. *Sep Purif Technol* 19(1–2):55–64. <http://hdl.handle.net/1783.1/24689>
26. Weber WJ, Morris JC (1963) Kinetics of adsorption on carbon from solution. *J Sanit Eng Div, Am Soc Civ Eng* 89(2):31–60
27. Dakrouy GA, Abo-Zahra ShF (2020) The use of titanium oxide/polyethylene glycol nanocomposite in sorption of ^{134}Cs and ^{60}Co radionuclides from aqueous solutions. *J Radioanal Nucl Chem* 324:1351–1364. <https://doi.org/10.1007/s10967-020-07167-9>
28. Lima EC, Hosseini-Bandegharai A, Moreno-Piraján JC, Anastopoulos I (2018) A critical review of the estimation of the thermodynamic parameters on adsorption equilibria. Wrong use of equilibrium constant in the Van't Hoof equation for calculation of thermodynamic parameters of adsorption. *J Mol Liq* 273:425–434. <https://doi.org/10.1016/j.molliq.2018.10.048>
29. Ayawei N, Ebelegi AN, Wankasi D (2017) Modelling and interpretation of adsorption isotherms. *J Chem* 2017:1–11. <https://doi.org/10.1155/2017/3039817>
30. Khezami L, Taha KK, Modwi A (2017) Efficient removal of cobalt from aqueous solution by zinc oxide nanoparticles: kinetic and thermodynamic studies". *Zeitschrift für Naturforschung* 72(5):409–418. <https://doi.org/10.1515/zna-2016-0477>
31. Lefatshe K, Muiva CM, Kebaabetswe LP (2017) Extraction of Nanocellulose and In-Situ Casting of ZnO/Cellulose Nanocomposite with Enhanced Photocatalytic and Antibacterial Activity. *Carbohydr Polym* 164:301–308. <https://doi.org/10.1016/j.carbpol.2017.02.020>
32. Abdelrehim MM, Mohy ElDin MH, El-Shabrawy SM, Fahmy AE, Abdelhamid SM, Ramadan HS (2019) Synthesis and characterization of metallic and polymeric nanoparticles and their effect on the antibacterial properties of microhybrid composite resin. *Alexandria Dental J Article* 7 44(2):39–45. <https://doi.org/10.21608/ADJAL.EXU.2019.57361>
33. Prokhorov E, Luna-Bárceñas G, Yáñez LJM, Sánchez AG, Kovalenko Y (2020) Chitosan-ZnO nanocomposites assessed by dielectric, mechanical, and piezoelectric properties. *Polymers* 12(9):1991–2005. <https://doi.org/10.3390/polym12091991>
34. Zak AK, Abd. Majid WH, Mahmoudian MR, Darroudi M, Yousefi R (2013) Starch-stabilized synthesis of ZnO nanopowders at low temperature and optical properties study. *Adv Powder Technol* 24(3):618–624. <https://doi.org/10.1016/j.apt.2012.11.008>
35. Sagadevan S, Vennila S, Anita Lett J, Marlinda AR, Aliya Binti Hamizi N, Rafie Johan M (2019) Tailoring the structural, morphological, optical, thermal and dielectric characteristics of ZnO nanoparticles using starch as a capping agent. *Results in Physics* 15 (2019) 102543 ISSN 2211-3797. <https://doi.org/10.1016/j.rinp.2019.102543>
36. Hassan HS, Attia LA, Dakrouy GA (2020) Exploration of the parameters affecting the radioactive europium removal from aqueous solutions by activated carbon-epoxy composite. *Appl Radiat Isot* 164:109278. <https://doi.org/10.1016/j.apradiso.2020.109278>
37. Puigdomenech I (2013) Make equilibrium diagrams using sophisticated algorithms (MEDUSA). Inorganic Chemistry Royal Institute of Technology Stockholm Sweden. <http://www.kemi.kth.se/medusa> <https://sites.google.com/site/chemdiagr/>
38. Hasan S, Iasir ARM, Ghosh TK, Gupta BS, Prelas MA (2019) Characterization and adsorption behavior of strontium from aqueous solutions onto chitosan-fuller's earth beads. *Healthcare* 7(1):52. <https://doi.org/10.3390/healthcare7010052>
39. Al-Senani GM, Al-Fawzan FF (2019) Adsorption study of heavy metal ions from aqueous solution by nanoparticle of wild herbs. *Egypt J Aquat Res* 44(3):187–194 ISSN 1687-4285, <https://doi.org/10.1016/j.ejar.2018.07.006>
40. Zhang N, Liu S, Jiang L, Luo M, Chi C, Ma J (2015) Adsorption of strontium from aqueous solution by silica mesoporous SBA-15. *J Radioanal Nucl Chem* 303:1671–1677. <https://doi.org/10.1007/s10967-014-3681-1>
41. Robati D (2013) Pseudo-second-order kinetic equations for modeling adsorption systems for removal of lead ions using multi-walled carbon nanotube. *J Nanostruct Chem* 3(1):55. <https://doi.org/10.1186/2193-8865-3-55>
42. Igwe JC, Abia AA (2007) Adsorption isotherm studies of Cd (II), Pb (II) and Zn (II) ions bioremediation from aqueous solution using unmodified and EDTA-modified maize cob. *Eclética Química* 32(1):33–42. <https://doi.org/10.1590/S0100-46702007000100005>
43. Li D, Zhang B, Xuan F (2015) The sequestration of Sr(II) and Cs(I) from aqueous solutions by magnetic graphene oxides. *J Mol Liq* 209:508–514. <https://doi.org/10.1016/j.molliq.2015.06.022>
44. Tan Y, Feng J, Qiu L, Zhao Z, Zhang X, Zhang H (2017) The adsorption of Sr(II) and Cs(I) ions by irradiated *Saccharomyces cerevisiae*. *J Radioanal Nucl Chem* 314:2271–2280. <https://doi.org/10.1007/s10967-017-5598-y>
45. Lee CH, Park JM, Lee MG (2014) Adsorption characteristics of Sr(II) and Cs(I) ions by zeolite synthesized from coal fly ash. *Int J Environ Sci* 23(12):1987–1998. <https://doi.org/10.5322/JESI.2014.23.12.1987>
46. Ali MMS, Sami NM, El-Sayed AA (2020) Removal of Cs⁺, Sr²⁺ and Co²⁺ by activated charcoal modified with Prussian blue nanoparticle (PBNP) from aqueous media: kinetics and equilibrium studies. *J Radioanal Nucl Chem* 324:189–201. <https://doi.org/10.1007/s10967-020-07067-y>
47. Chen C, Wang J (2008) Removal of Pb²⁺, As⁺, Cs⁺ and Sr²⁺ from aqueous solution by brewery's waste biomass. *J Hazard Mater* 151:65–70. <https://doi.org/10.1016/j.jhazmat.2007.05.046>
48. Uematsu Y, Ogata F, Saenjum C, Nakamura T, Kawasaki N (2020) Removing Sr(II) and Cs(I) from the aqueous phase using basil seed and elucidating the adsorption mechanism. *Sustainability* 12(7):2895. <https://doi.org/10.3390/su12072895>

Publisher's Note Springer Nature remains neutral with regard to jurisdictional claims in published maps and institutional affiliations.